Nanostructures

DOI: 10.1002/anie.201107838

A Nanosheet-Structured Three-Dimensional Macroporous Material with High Ionic Conductivity Synthesized Using Glucose as a Transforming Template**

*Junjie Ge, Hanping Ding, and Xingjian Xue**

The advancements of both top-down and bottom-up synthesis strategies have yielded very interesting findings towards the synthesis of nanosheets.[1] The preparation of nanosheets with top-down methods typically involves the exfoliation of layer-structured materials. Examples include the nanosheet synthesis of transition-metal dichalcogenides (TMDs), transition-metal oxides (TMOs), and compounds such as BN, Bi_2Te_3, and Bi_2Se_3.[1a,2] As the parent layered compound is the essential requirement for exfoliations, nanosheet synthesis for the materials without layered structures have been excluded from the top-down method. On the other hand, the bottom-up method also presents difficulties in the synthesis of nanosheet materials with structures other than layered compounds, such as cubic structures, because of the lack of intrinsic driving force for two-dimensional (2D) growth.[1d] Furthermore, the existing methods are not readily scaled up for large quantity preparations. Clearly, a method that can produce large scale nanosheets for a wide variety of materials is of particular significance.

Ceria has found application in catalysis, solid oxide fuel cells, and oxygen sensors.[3] In particular, when ceria is doped with other rare-earth ions, it can significantly increase the oxygen vacancies and ionic conductivities.[4] Zero- and one-dimensional ceria-based nanocrystals have been investigated using different approaches.[5] However, it is difficult to achieve 2D structured ceria-based materials owing to their face-centered cubic structure (Figure 1 a).[1d]

Glucose has been used as a source for carbon materials, as it is readily available, environmentally benign, and easy to control.[6] Upon heating in air, glucose undergoes successive reactions, that is, polymerization, carbonization, and combustion. Inspired by this feature, a novel simple one-pot glucose combustion route was devised to synthesize inorganic compounds with $Sm_{0.2}Ce_{0.8}O_{1.9}$ (SDC) as an example. The glucose acts as both the fuel and a transforming template, leading to the formation of three-dimensional (3D) macroporous SDC with a 2D nanosheet microstructure. To our best knowledge, this microstructure was achieved for the first time.

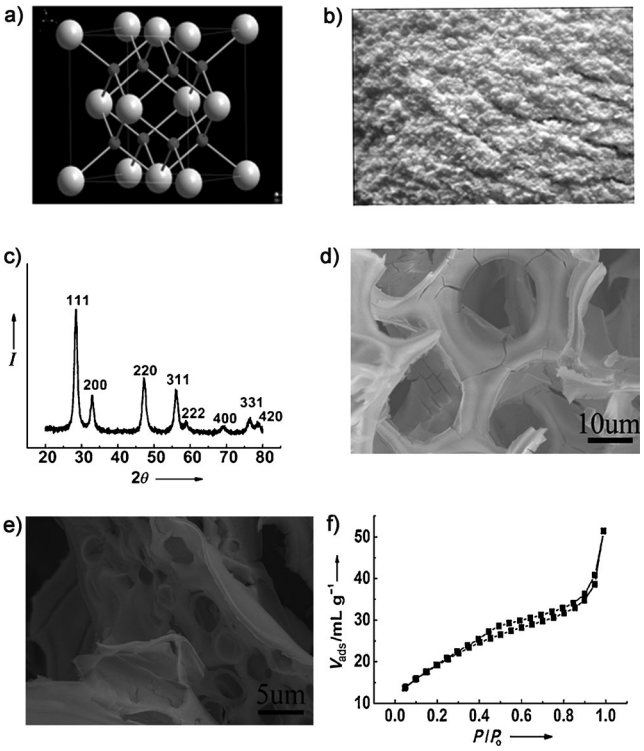

Figure 1. a) The unit cell of ceria with a fluorite structure; b) porous SDC powders obtained by the glucose combustion method; c) the XRD pattern of the sample; d), e) SEM images of the sample; f) a nitrogen adsorption/desorption isotherm of the sample.

The SDC sample prepared through the combustion process is shown in Figure 1 b; free-flowing yellow powders were obtained. The filled density of the SDC powders was as low as 0.020 g cm^{-3}, which is only 0.28 % of the theoretical density (7.15 g cm^{-3}) of the bulk SDC. Equivalently, the apparent volume of this SDC powder is about 357 times that of the same amount of bulk material. In general, materials produced through wet chemistry methods[1e,2] are dispersed in solvents; therefore, complicated separation processes are needed to obtain the solid materials, and agglomerations may occur. The combustion method shown herein offers a simple way to produce porous solid powders directly in large scales. The powder X-ray diffraction (XRD) pattern (Figure 1 c) confirmed that the synthesized SDC sample exhibits the single-phase cubic fluorite structure ($Fm\bar{3}m$; JCPDS card no. 34-394). The strong peak intensity indicates that the sample

[*] Dr. J. Ge, H. Ding, Prof. X. Xue
Department of Mechanical Engineering
University of South Carolina, Columbia, SC 29208 (USA)
E-mail: xue@cec.sc.edu

[**] We thank NSF, grant no. CMMI-1000068, grant no. CMMI-1100085, US DOE Basic Energy Sciences, grant no. DE-SC0001061, and the University of South Carolina, Office of Research and Graduate Education for financial support.

Supporting information for this article is available on the WWW under http://dx.doi.org/10.1002/anie.201107838.

was crystalline. The lattice parameter calculated was 5.4352 Å and the *d* spacing values with the peaks of (111), (200), (220), and (311) were 3.1381, 2.7202, 1.9216, and 1.6372 Å, respectively. The lattice parameter and *d* spacing values are larger than those from the JCPDS, demonstrating that the crystal unit cell was expanded. This expansion is induced by the fact that some of the Ce^{4+} ions with a smaller radius of 0.0971 nm were replaced by Sm^{3+} with a larger radius of 0.1079 nm.[4] Figure 1 d,e show the FESEM images of the SDC sample in different areas. Both images show 3D macroporous architectures. Hollow-type pores are observed, with diameters ranging from a few micrometers to several dozens of micrometers. The wall of the 3D structure shown is continuous with a few cracks being observed. The sheet structure can be observed in Figure 1 d,e and was further confirmed by TEM. The nitrogen adsorption and desorption results (Figure 1 f) exhibit a type II isotherm, which is typical for nonporous and macroporous materials. The Brunauer–Emmett–Teller (BET) calculation showed that the specific surface area of the SDC sample is as high as 68.94 $m^2 g^{-1}$. To illustrate the difference between the glucose combustion method and other methods, the widely used citrate–nitrate combustion route was adopted to prepare SDC powders. As shown in the Supporting Information, Figure S1, a foamy structure with irregular pores was obtained, which is similar to the powders obtained with other fuels.[7] The powders showed single-phase cubic fluorite structure; however, the specific surface area (34.67 $m^2 g^{-1}$) was only half that of the powders from the glucose method under the same calcination temperature (500 °C; Supporting Information, Figures S2, S3).

Figure 2 a and Figure S4 (Supporting Information) show the representative TEM images of the synthesized SDC nanosheets. The nanosheets are composed of connected nanoparticles with lateral dimension up to micrometers. Upon continuous sonication, some multilayer nanosheets were delaminated and the single layer nanosheets were obtained. Figure 2 b shows the partially separated mutilayers of the nanosheets, while Figure 2 c,d present the well-defined single-layered SDC nanosheets, as observed from the side view. The single-layered nanosheets are composed of 2D network of interconnected nanoparticles with an average particle diameter of approximately 4 nm. Therefore, the average thickness of a single-layer nanosheet is also around 4 nm. Interestingly, some of the nanosheets appeared to be wrinkled (Figure 2 c), self-folded (Figure 2 d), and even rolled into cylindrical structures (Figure 2 e), demonstrating that the synthesized nanosheets are elastic in nature and are capable of transforming into versatile structures. Using TEM, the nanosheets were estimated to account for more than 95 % of the total amount of the SDC products. A selected-area electron diffraction (SAED) pattern (Figure 2 f) reveals the polycrystalline nature of the nanosheets, which is consistent with the results from TEM. Nanosheets with other compositions, such as CeO_2 and $La_{0.6}Sr_{0.4}Co_{0.2}Fe_{0.8}O_{3-\delta}$, were also synthesized using the same route (Supporting Information, Figure S5 and Figure S6, respectively), demonstrating the generality of this approach for the synthesis of nanosheet-structured inorganic materials. The TEM image of the powders from the citrate–nitrate method is shown in the Supporting Information, Figure S7; nanoaggregates with particle sizes ranging from 3 nm to 15 nm were observed.

Figure 3 a illustrates the mechanism on transforming the glucose and metal precursors into the final SDC product. First, a solution containing glucose and metal precusors was heat-treated, excessive water was evaporated from the system, and the polymerization of glucose took place, as indicated by both the solution color change and viscosity increase. The polymerization process leads to the formation of a continuous frame, which was subsequently transformed into carbon. A uniform composite was formed owing to the chelation between metal ions and the functional groups of glucose and polymerized glucose (that is, OH and −C=O). Under high-temperature conditions, the carbonization of the

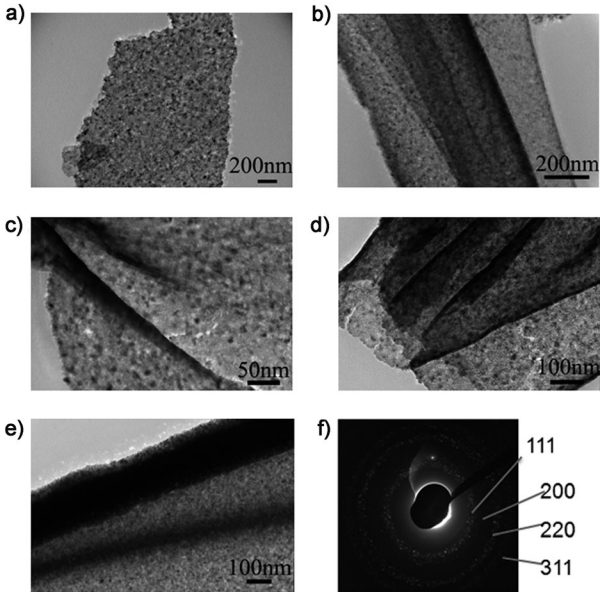

Figure 2. a)–e) TEM and the f) SAED images for the sample.

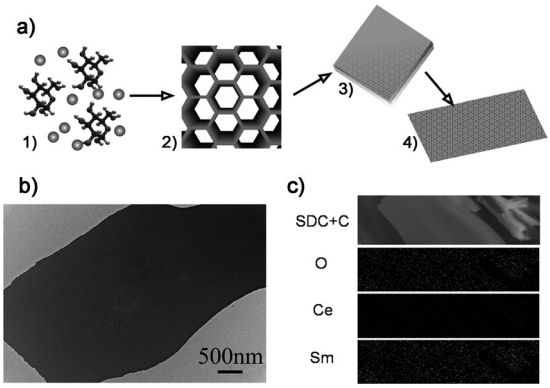

Figure 3. a) Formation mechanism of nanosheet structure: 1) A mixed solution containing glucose and metal nitrates; 2) formation of 3D macroporous composites composed of SDC and carbon; 3) the wall of the 3D composite shown in (2) in which SDC is embedded in the carbon material to form composite nanosheets; 4) the SDC nanosheet formed after the carbon was burnt off. b) TEM characterization of the SDC/C composite. c) FESEM and EDX map characterization of the SDC/C composite.

glucose and the decomposition of metal nitrates occurred, producing a large amount of gas-phase compounds. The continuous carbon structure in combination with the large amount of gas production formed the composite structure into 3D macroporous SDC/carbon composite (SDC/C) with continuous walls, as shown in process (2) of Figure 3a. As a reaction intermediate, the SDC/C composite was synthesized under the protection of nitrogen and investigated using various physical characterization techniques. Figure S8 (Supporting Information) confirms the 3D macroporous structure of the obtained SDC/C composite. The SDC/C composite was assembled into a 2D sheet structure, as shown in both Figure 3b (TEM) and the Supporting Information, Figure S9 (FESEM). The structure is most likely due to the ordered polymerization of glucose. To verify this proposal, the glucose was heat-treated individually without the involvement of metal precursors, and a similar nanosheet structure was observed as shown in the Supporting Information, Figure S10. The status of SDC in the composite was characterized by XRD (Supporting Information, Figure S11) and the energy-dispersive X-ray (EDX map) combined with FESEM (Figure 3c). The EDX map results show that Ce, Sm, and O were all uniformly dispersed in the sheets, while XRD only shows diffraction peaks corresponding to graphite. The above results suggest that SDC was formed in ultrasmall crystal size (SDC nuclei) embedded in the carbon matrix. The homogeneous distribution and small crystal size of SDC strongly indicate the uniform chelation of the metal precusors to glucose and the strong protection effect of the carbon matrix. With a further increase in temperature, combustion took place and carbon left the system in the form of carbon dioxide. Meanwhile, the adjacent SDC nuclei condensed together to form connected nanocrystals with larger size and reproduced the sheet structure of the carbon matrix. Through these processes, 3D macroporous SDC with a 2D nanosheet microstructure was synthesized, with glucose acting as a transforming template.

The inorganic materials with nanosheet structures have potential applications in photocatalysis, electronic devices, light-emitting devices, solar cells, bioimaging, and biosensors.[8] As an ionic conducting material, SDC membranes fabricated from 0D and 1D nanomaterials have shown enhanced conductivity owing to the different sintering properties of those polycrystalline powders and/or an increase in the density of mobile defects in the space-charge region.[5b–d] Here the synthesized nanosheet-structured powders were studied for electrolyte fabrications. Shown in Figure 4a is the SEM image of a green pellet obtained by uniaxially dry-pressing the synthesized 2D nano-SDC powder. The SDC nanosheets are packed together compactly and uniformly in parallel, resulting in a pellet with a relatively smooth surface. The nanosheets intertwine with each other within the dry-pressed pellet (Figure 4a and Supporting Information, Figure S12), making it relatively easy to form a gas-tight membrane. Figure S13–S15 (Supporting Information) present the surface SEM images of the pellets sintered at different temperatures. At a sintering temperature of 1300 °C, the grain size grew and formed an obvious grain boundary within the individual nanosheets. However, the bonding

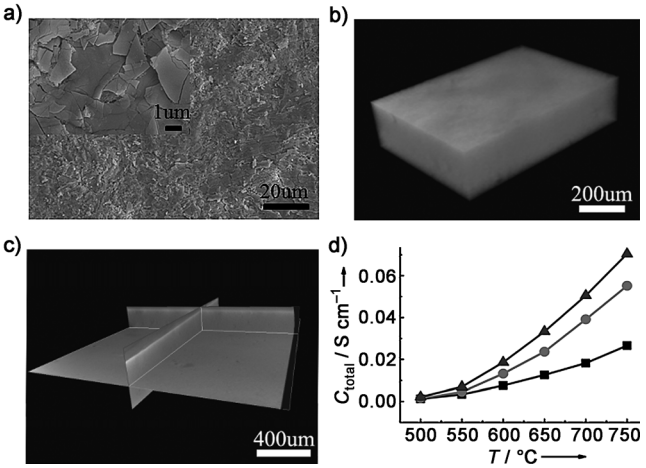

Figure 4. a) SEM image of the dry pressed pellets before sintering; b) an XCT image of the SDC pellet sintered at 1500 °C; c) a cross-sectional view of XCT image for the pellet sintered at 1500 °C; d) the total conductivity C_{total} versus measuring temperature T for the pellets sintered at ■ 1300 °C, ● 1400 °C, and ▲ 1500 °C.

between the nanosheets was not well established (Supporting Information, Figure S13). When sintered at 1400 °C, larger grain size with improved inter-nanosheet bonding was observed (Supporting Information, Figure S14). With the further increase of sintering temperature to 1500 °C, the clear inter-nanosheet boundaries disappeared with significant grain-size growth (Supporting Information, Figure S15). The relative density of the pellets sintered at 1400 °C and 1500 °C was calculated to be 98.0 % and 99.3 %, respectively. The 3D X-ray computed tomography imaging (XCT) technique was used to investigate the detailed internal structures of the membranes. The internal structures of the pellets after sintering at different temperatures are shown in the Supporting Information, Figures S16, S17. With increasing the sintering temperature, denser pellets were obtained. The XCT images in Figure 4b,c further confirmed the dense SDC structure sintered at 1500 °C. Figure 4d shows the total conductivity of SDC pellets in air as the function of the measuring temperature. The conductivity of all the pellets increases with increasing the measuring temperatures owing to the transference of oxygen vacancy, and shows the semiconducting nature of SDC.[9] Under the same measuring temperature above 500 °C, the conductivity increases with increasing the sintering temperatures. The total conductivity is contributed from both the grain interior (gi) and grain boundary (gb). As shown in the Supporting Information, Figure S18, both the resistance of grain boundary (Rgb) and that of grain interior (Rgi) decreases upon increasing the sintering temperature. However, the decrease in Rgb is more remarkable and has dominant influence on the total conductivity. Rgb is related to the volume fraction of grain boundaries, while the pellet sintered at higher temperatures has larger grain size and a decreased volume fraction of grain boundaries, resulting in decreased grain boundary resistance. As shown in the Supporting Information, Figure S15, the pellet sintered at 1500 °C exhibited a grain size up to 10 μm, and therefore showed the highest total conductivity (Fig-

ure 4d). The sintering performance of the nanopowders from the citrate–nitrate method is shown in the Supporting Information, Figure S19–21. The average grain size increased with an increased sintering temperature, from less than 1 μm at 1300 °C to around 2 μm at 1500 °C. The relative pellet density sintered at 1400 °C and 1500 °C was calculated to be 95.2 % and 98.5 %, respectively. Obviously under the same sintering conditions, the pellets from nanosheet structure had larger grain size and higher bulk density than those of the pellets from citrate–nitrate nanopowders, indicating better sinterability of the former. Accordingly, the nanosheet pellet sintered at 1500 °C exhibited the conductivity of 0.051 $S\,cm^{-1}$ and 0.019 $S\,cm^{-1}$ at 700 °C and 600 °C, respectively. However, with the same sintering condition, the pellet from citrate nitrate nanoaggregates showed the conductivity of 0.036 $S\,cm^{-1}$ at 700 °C and 0.012 $S\,cm^{-1}$ at 600 °C, respectively (Supporting Information, Figure S22). Similar conductivity has been obtained (0.031 $S\,cm^{-1}$ at 700 °C and 0.01 $S\,cm^{-1}$ at 600 °C) when fine nanoparticles were used to fabricate the membrane.[4]

In summary, a novel combustion route has been developed to synthesize 3D macroporous SDC with a 2D nanosheet microstructure in which the glucose acts as both the fuel and a transforming template. The developed combustion synthesis route is simple, highly reliable, and easily scaled up. The SDC nanosheets obtained have the single layer thickness of 4 nm and lateral dimension of up to several micrometers. The SDC powder with a nanosheet structure exhibits great advantages in fabricating dense and highly conductive electrolyte membranes. The developed approach is generic and can be readily extended to the synthesis of other nanosheet-structured metal oxides and compounds.

Experimental Section

Synthesis of SDC: $Ce(NO_3)_3{\cdot}6H_2O$ (3.68 g, 8.47 mmol), $Sm(NO_3)_3{\cdot}6H_2O$ (0.942 g, 2.12 mmol), and glucose (10 g, 55.51 mmol) were dissolved together in water (50 mL). The solution was heated on a hot plate until it ignited with flames. The resulting lightly yellow powder was calcined at 500 °C to form the pure SDC crystalline. The SDC and carbon composite were also synthesized under N_2. First, the mixed solution of the glucose and metal oxide precursors was heated on the hot plate until the solution became viscous and the color turned into orange, which indicates the occurrence of the polymerization. The solution was cooled and transformed into one solid piece. Subsequently it was heated to 600 °C for 3 h in a furnace to obtain the SDC/C composite under N_2. The electrolyte pellets were prepared using uniaxial dry-pressing method. SDC nanopowder (0.3 g) was put into a cylindrical stainless steel die with a 15 mm diameter and dry-pressed at 200MPa to form a pellet. The pellets were sintered in air for 5 h at 1300 °C, 1400 °C, and 1500 °C.

Received: November 7, 2011
Revised: March 5, 2012
Published online: May 4, 2012

Keywords: ceramics · ionic conductors · macroporous structures · nanosheets · nanostructures

[1] a) J. N. Coleman, M. Lotya, A. O'Neill, S. D. Bergin, P. J. King, U. Khan, K. Young, A. Gaucher, S. De, R. J. Smith, I. V. Shvets, S. K. Arora, G. Stanton, H. Y. Kim, K. Lee, G. T. Kim, G. S. Duesberg, T. Hallam, J. J. Boland, J. J. Wang, J. F. Donegan, J. C. Grunlan, G. Moriarty, A. Shmeliov, R. J. Nicholls, J. M. Perkins, E. M. Grieveson, K. Theuwissen, D. W. McComb, P. D. Nellist, V. Nicolosi, *Science* **2011**, *331*, 568–571; b) X. Liu, R. Ma, Y. Bando, T. Sasaki, *Angew. Chem.* **2010**, *122*, 8429–8432; *Angew. Chem. Int. Ed.* **2010**, *49*, 8253–8256; c) S. Ida, C. Ogata, M. Eguchi, W. J. Youngblood, T. E. Mallouk, Y. Matsumoto, *J. Am. Chem. Soc.* **2008**, *130*, 7052–7059; d) T. Yu, B. Lim, Y. Xia, *Angew. Chem.* **2010**, *122*, 4586–4589; *Angew. Chem. Int. Ed.* **2010**, *49*, 4484–4487; e) D. D. Vaughn II, R. J. Patel, M. A. Hickner, R. E. Schaak, *J. Am. Chem. Soc.* **2010**, *132*, 15170–15172; f) J.-w. Seo, Y.-w. Jun, S.-w. Park, H. Nah, T. Moon, B. Park, J.-G. Kim, Y. J. Kim, J. Cheon, *Angew. Chem.* **2007**, *119*, 8984–8987; *Angew. Chem. Int. Ed.* **2007**, *46*, 8828–8831; g) J. S. Son, X.-D. Wen, J. Joo, J. Chae, S.-i. Baek, K. Park, J. H. Kim, K. An, J. H. Yu, S. G. Kwon, S.-H. Choi, Z. Wang, Y.-W. Kim, Y. Kuk, R. Hoffmann, T. Hyeon, *Angew. Chem.* **2009**, *121*, 6993–6996; *Angew. Chem. Int. Ed.* **2009**, *48*, 6861–6864.

[2] Y. Matsumoto, M. Koinuma, Y. Iwanaga, T. Sato, S. Ida, *J. Am. Chem. Soc.* **2009**, *131*, 6644–6645.

[3] a) F. Yang, J. s. Graciani, J. Evans, P. Liu, J. Hrbek, J. F. Sanz, J. A. Rodriguez, *J. Am. Chem. Soc.* **2011**, *133*, 3444–3451; b) P. Gao, Z. Kang, W. Fu, W. Wang, X. Bai, E. Wang, *J. Am. Chem. Soc.* **2010**, *132*, 4197–4201; c) T. Montini, A. Speghini, L. D. Rogatis, B. Lorenzut, M. Bettinelli, M. Graziani, P. Fornasiero, *J. Am. Chem. Soc.* **2009**, *131*, 13155–13160.

[4] Q. Liu, F. Zhao, X. H. Dong, C. H. Yang, F. L. Chen, *J. Phys. Chem. C* **2009**, *113*, 17262–17267.

[5] a) X. Liu, K. Zhou, L. Wang, B. Wang, Y. Li, *J. Am. Chem. Soc.* **2009**, *131*, 3140–3141; b) Y. Ma, X. D. Wang, S. H. Li, M. S. Toprak, B. Zhu, M. Muhammed, *Adv. Mater.* **2010**, *22*, 1640–1644; c) Y. B. Go, A. J. Jacobson, *Chem. Mater.* **2007**, *19*, 4702–4709; d) T. Karaca, T. G. Altincekic, M. F. Oksuzomer, *Ceram. Int.* **2010**, *36*, 1101–1107.

[6] a) G. B. Yu, B. Sun, Y. Pei, S. H. Xie, S. R. Yan, M. H. Qiao, K. N. Fan, X. X. Zhang, B. N. Zong, *J. Am. Chem. Soc.* **2010**, *132*, 935–937; b) S. E. Chun, Y. N. Picard, J. F. Whitacre, *J. Electrochem. Soc.* **2011**, *158*, A83–A92.

[7] C. Xia, Y. Li, Y. Tian, Q. H. Liu, Z. M. Wang, L. J. Jia, Y. C. Zhao, Y. D. Li, *J. Power Sources* **2010**, *195*, 3149–3154.

[8] a) J. A. Gerbec, D. Magana, A. Washington, G. F. Strouse, *J. Am. Chem. Soc.* **2005**, *127*, 15791–15800; b) K. J. Tang, J. N. Zhang, W. F. Yan, Z. H. Li, Y. D. Wang, W. M. Yang, Z. K. Xie, T. L. Sun, H. Fuchs, *J. Am. Chem. Soc.* **2008**, *130*, 2676–2680.

[9] B. B. Patil, S. H. Pawar, *Appl. Surf. Sci.* **2007**, *253*, 4994–5002.

